

University of Groningen

Asymmetric synthesis of optically pure aliphatic amines with an engineered robust ω -transaminase

Dong, Linhan; Meng, Qinglong; Ramirez-Palacios, Carlos; Wijma, Hein J.; Marrink, Siewert J.; Janssen, Dick B.

Published in:
Catalysts

DOI:
[10.3390/catal10111310](https://doi.org/10.3390/catal10111310)

IMPORTANT NOTE: You are advised to consult the publisher's version (publisher's PDF) if you wish to cite from it. Please check the document version below.

Document Version
Publisher's PDF, also known as Version of record

Publication date:
2020

[Link to publication in University of Groningen/UMCG research database](#)

Citation for published version (APA):

Dong, L., Meng, Q., Ramirez-Palacios, C., Wijma, H. J., Marrink, S. J., & Janssen, D. B. (2020). Asymmetric synthesis of optically pure aliphatic amines with an engineered robust ω -transaminase. *Catalysts*, 10(11), 1-14. [1310]. <https://doi.org/10.3390/catal10111310>

Copyright

Other than for strictly personal use, it is not permitted to download or to forward/distribute the text or part of it without the consent of the author(s) and/or copyright holder(s), unless the work is under an open content license (like Creative Commons).

The publication may also be distributed here under the terms of Article 25fa of the Dutch Copyright Act, indicated by the "Taverne" license. More information can be found on the University of Groningen website: <https://www.rug.nl/library/open-access/self-archiving-pure/taverne-amendment>.

Take-down policy

If you believe that this document breaches copyright please contact us providing details, and we will remove access to the work immediately and investigate your claim.

Downloaded from the University of Groningen/UMCG research database (Pure): <http://www.rug.nl/research/portal>. For technical reasons the number of authors shown on this cover page is limited to 10 maximum.

Article

Asymmetric Synthesis of Optically Pure Aliphatic Amines with an Engineered Robust ω -Transaminase

Linhan Dong^{1,2}, Qinglong Meng¹, Carlos Ramírez-Palacios^{1,3} , Hein J. Wijma¹ ,
Siewert J. Marrink³  and Dick B. Janssen^{1,*}

¹ Biotransformation and Biocatalysis Group, Groningen Biomolecular Sciences and Biotechnology Institute (GBB), University of Groningen, Nijenborgh 4, 9747 AG Groningen, The Netherlands; donglinhan1998@gmail.com (L.D.); q.meng@rug.nl (Q.M.); j.c.ramirez.palacios@rug.nl (C.R.-P.); h.j.wijma@rug.nl (H.J.W.)

² College of Chemistry, Jilin University, 2699 Qianjin Avenue, Changchun 130012, China

³ Molecular Dynamics Group, Groningen Biomolecular Sciences and Biotechnology Institute (GBB), University of Groningen, Nijenborgh 7, 9747 AG Groningen, The Netherlands; s.j.marrink@rug.nl

* Correspondence: d.b.janssen@rug.nl; Tel.: +31-503-634-008

Received: 12 October 2020; Accepted: 8 November 2020; Published: 12 November 2020



Abstract: The production of chiral amines by transaminase-catalyzed amination of ketones is an important application of biocatalysis in synthetic chemistry. It requires transaminases that show high enantioselectivity in asymmetric conversion of the ketone precursors. A robust derivative of ω -transaminase from *Pseudomonas jessenii* (*PjTA-R6*) that naturally acts on aliphatic substrates was constructed previously by our group. Here, we explore the catalytic potential of this thermostable enzyme for the synthesis of optically pure aliphatic amines and compare it to the well-studied transaminases from *Vibrio fluvialis* (*VfTA*) and *Chromobacterium violaceum* (*CvTA*). The product yields indicated improved performance of *PjTA-R6* over the other transaminases, and in most cases, the optical purity of the produced amine was above 99% enantiomeric excess (e.e.). Structural analysis revealed that the substrate binding poses were influenced and restricted by the switching arginine and that this accounted for differences in substrate specificities. Rosetta docking calculations with external aldimine structures showed a correlation between docking scores and synthetic yields. The results show that *PjTA-R6* is a promising biocatalyst for the asymmetric synthesis of aliphatic amines with a product spectrum that can be explained by its structural features.

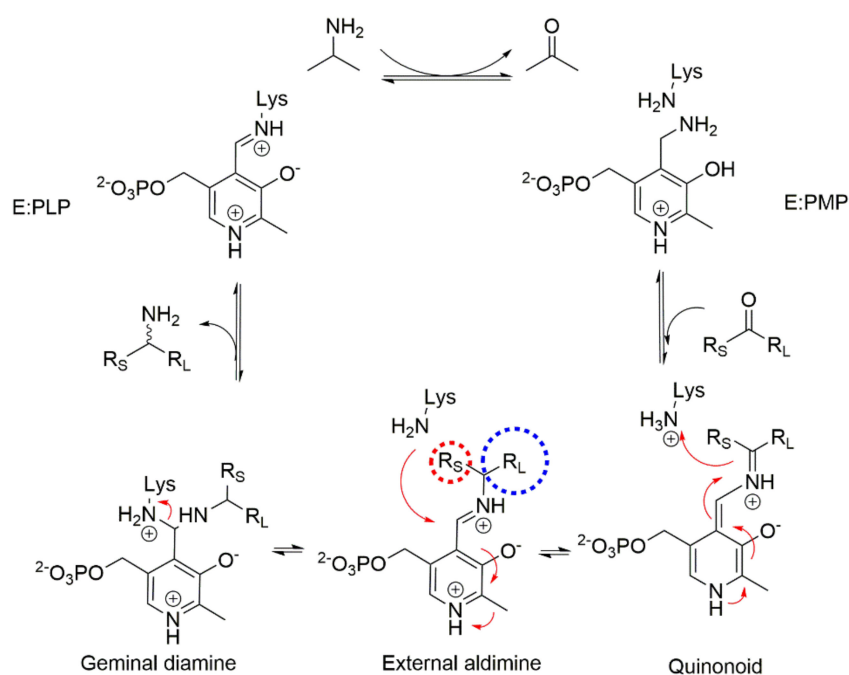
Keywords: transamination; asymmetric synthesis; alkanamines; transaminase; computational modeling

1. Introduction

Optically pure amines are of great interest for the pharmaceutical and wider fine chemical industries as they can serve as intermediates in the preparation of a diversity of biologically active compounds [1–3]. For example, chiral amines are used as building blocks in the synthesis of pharmaceuticals used in the treatment of Alzheimer's disease [4] and malaria [5] or as antitumor agents [6]. The enzymatic production of such amines is widely studied for furthering the application of biocatalysis in environmentally benign synthetic processes [7,8].

Transaminases (TAs) catalyze the transfer of amino groups from amines (amino donors) to aldehydes or ketones (amino acceptors), with pyridoxal-5' phosphate (PLP) as the cofactor (Scheme 1) [2,9]. Whereas α -transaminases act on substrates bearing a carboxylate group flanking the carbon carrying the amine functionality that is exchanged, ω -transaminases (ω -TAs) act on nonproteinogenic amino acids with the amine and carboxylate groups at terminal positions. Many ω -TAs and related enzymes are called amine transaminases (ATAs) as they act on substrates that lack a

carboxylate functionality. This relaxed substrate specificity allows amination of various ketones when added as amino acceptor [10]. Mechanistically, in the first half reaction, the amino donor aminates the PLP to form a pyridoxamine intermediate (PMP) in several proton transfer steps. In the second half reaction, the ketone acceptor binds to the PMP enzyme to form the aminated product and regenerate PLP (Scheme 1). Recent efforts to tailor the ω -TA substrate scope have focused on stabilization of the Michaelis complex of the ketone substrate [11–14] with little or no attention to reaction intermediates. The external aldimine is a key intermediate in the transamination reaction. Depending on the half reaction under consideration, the external aldimine can either undergo proton abstraction by the catalytic lysine to form a quinonoid intermediate or abstract a proton from lysine to form a geminal diamine intermediate [15]. Both formation and conversion of the external aldimine go through the formation of high-energy transition state structures, and their corresponding reactions are rate-limiting. Therefore, we hypothesized that substrates capable of forming more stable external aldimine complexes would overall have better reactivities.



Scheme 1. ω -Transaminase-catalyzed transamination with isopropylamine as the amino donor. The aldehyde/ketone substrate will bind to the pyridoxamine intermediate (PMP) enzyme to form an external aldimine. The relatively large (R_L) or small (R_S) ketone/amine rest groups are accommodated in the large or small binding pockets of the transaminase. The excess of isopropylamine drives the equilibrium toward the production of the target amine.

Prior work on the catalytic abilities of ω -TAs indicates versatile substrate spectra and (*S*)- or (*R*)-enantioenrichment of amines formed by conversion of prochiral ketones [16]. Compared with traditional chemical synthesis, harsh conditions and heavy metal catalysts are avoided by enzymatic reactions, displaying the green aspects of biocatalysis [3,7]. Moreover, the use of cheap amine donors or regeneration of the amine donor in TA-catalyzed amination enables one-pot asymmetric synthesis [3,17]. Therefore, the production of optically pure amines applying ω -TAs is considered promising from an application point of view. A large variety of transaminases that are active in the enzymatic synthesis of aromatic amines have been described [16]. In comparison, biocatalytic synthesis of chiral aliphatic amines is not well studied, and reports on asymmetric synthesis of aliphatic amines by TAs are scarce [16]. Nonetheless, aliphatic amines are frequently seen as important intermediates of pharmaceuticals and other biologically active compounds [7,18]. Thus, transaminases

capable of producing various enantiopure aliphatic amines would diversify and strengthen the biocatalytic toolbox.

Apart from the need for an active enzyme for aliphatic amine synthesis, there are also several technical challenges concerning TA-catalyzed amine production. First, the reaction equilibrium needs to be shifted from the amino donor toward the production of the target amines. Often, this is achieved using an excess of the amino donor, sometimes accompanied by the removal of the side product [7,16,19,20]. Second, to use and fully dissolve a high concentration of the ketone substrate that should undergo amination, a cosolvent is sometimes added [1,21]. Besides overcoming equilibrium issues, the reaction rate may need to be accelerated using a high temperature. The availability of a robust ω -TA is desired in such scenarios of high amino donor concentrations, presence of cosolvents, and high reaction temperatures [3].

The discovery [22] and characterization [23] of a class III (S)-selective ω -TA from *Pseudomonas jessenii* (*PjTA*) were described previously. Identified as a key enzyme in the caprolactam degradation pathway of *P. jessenii*, *PjTA* converts 6-aminohexanoic acid (6-AHA) to 6-oxohexanoic acid (6-OHA). Our group has deepened the understanding of this enzyme by solving crystal structures and measuring its activities using over 40 different amine substrates [23]. A robust six-fold mutant of *PjTA* (*PjTA*-R6) was recently constructed using a framework for rapid enzyme stabilization by computational library design (FRESCO) [24]. The natural substrate of *PjTA* is a linear aliphatic ω -amino acid, which suggests *PjTA* may have potential for the synthesis of aliphatic amines. Moreover, the robust mutant *PjTA*-R6 is expected to tolerate a high concentration of amino donor, the presence of cosolvent, and an enhanced reaction temperature [24]. Thus, in the work reported here, we explored *PjTA*-R6 for the synthesis of aliphatic amines for which the wild-type *PjTA* was not considered as attractive due to its lower stability under harsh conditions. Considering their structural diversity and similarity to pharmaceutical building blocks, 10 aliphatic amines were selected for enzymatic production [8,18]. This included two amines with cycloalkyl substituents (**C1** and **C2** in Table 1).

Table 1. Analytical yields and enantiomeric excesses for the production of **A1–A5**, **B1–B3**, and **C1–C2** using a six-fold mutant of transaminase from *Pseudomonas jessenii* (*PjTA*-R6), a transaminase from *Chromobacterium violaceum* (*CvTA*), and a transaminase from *Vibrio fluvialis* (*VfTA*).¹

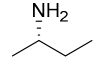
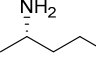
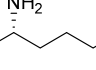
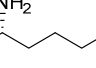
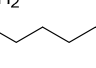
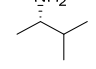
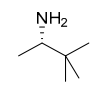
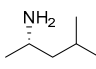
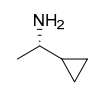
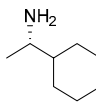
Amine Target Code	Amine Structure	<i>PjTA</i> -R6		<i>CvTA</i>		<i>VfTA</i>	
		Yield ¹ (%)	e.e. ² (%)	Yield (%)	e.e. (%)	Yield (%)	e.e. (%)
A1		70	94	40	86	5	n.d. ³
A2		80	98	34	91	12	41
A3		51	>99	23	91	14	88
A4		51	>99	44	90	41	92
A5		42	>99	46	88	35	94
B1		95	>99	3	n.d.	1	n.d.

Table 1. Cont.

Amine Target Code	Amine Structure	<i>PjTA-R6</i>		<i>CvTA</i>		<i>VfTA</i>	
		Yield ¹ (%)	e.e. ² (%)	Yield (%)	e.e. (%)	Yield (%)	e.e. (%)
B2		81	>99	3	n.d.	2	n.d.
B3		48	>99	<1	n.d.	2	n.d.
C1		42	>99	1	n.d.	<1	n.d.
C2		63	>99	<1	n.d.	1	n.d.

Reaction conditions: 1 mL volume, 20 mM ketone substrate, 1 M isopropylamine, 0.5 mM pyridoxal-5' phosphate (PLP), 1 mg/mL purified transaminase, 2% dimethyl sulfoxide (DMSO) (20% for A5), 20 h, 56 °C for *PjTA-R6* and 37 °C for *CvTA* and *VfTA*. ¹ The yields obtained with *PjTA-R6* are the averages of duplicates that differed less than 10%. ² e.e.: enantiomeric excess. ³ n.d.: not determined. enzymes. Noticeably, after 20 h of reaction, an enzyme precipitate was observed in the vials containing *CvTA* and *VfTA* but not in the reaction mixtures containing *PjTA-R6*. This agreed with our expectation that *PjTA-R6* would be more robust than the other two transaminases at high reaction temperature with excess amino donor present.

To compare the performance of *PjAT-R6* to other well-characterized (*S*)-selective TAs, we included the enzymes from *Chromobacterium violaceum* (*CvTA*) and *Vibrio fluvialis* (*VfTA*). Through a systematic analysis of the substrate spectrum of various transaminases reported in different papers, Calvelage et al. [25] concluded that *CvTA* and *VfTA* have advantages in converting straight-chain amines over other transaminases. The relative performance of *PjTA-R6* in comparison to *CvTA* and *VfTA* may help to evaluate the enzyme in terms of its significance within the enzymatic toolbox. Under the employed conditions, the yields of aliphatic amines obtained with *PjTA-R6* were higher than with *CvTA* or *VfTA*, and the enantiopurity of the produced amines was also higher.

Aiming to understand the structural basis for the observed reactivities of *PjTA-R6* and *VfTA*, we performed docking calculations of the external aldimine complexes of the tested substrates. For both enzymes, the interface energies of the external aldimine complexes correlated well with experimental reaction yields, indicating that biocatalytic scope can be accessed computationally for further redesign attempts. The docking complexes hinted to pivotal structural differences in the way *PjTA-R6* and *VfTA* accommodate bulky or alkyl chains in the large substrate binding pocket.

2. Results and Discussion

2.1. Asymmetric Synthesis of Aliphatic Amines

To investigate the performance of *PjTA-R6* in the asymmetric synthesis of aliphatic amines and compare the results with *CvTA* and *VfTA*, amination reactions were conducted using the three enzymes and a series of keto substrates (Table 1). For these amination reactions, we adopted conditions with a 50-fold excess of isopropylamine (IPA) as the amino donor (Scheme 1). This amino donor is relatively cheap [7] and highly water soluble, making its use in enzymatic aminations economically attractive. Moreover, IPA is transformed to acetone, whose volatility may simplify the work-up procedure [26]. The reaction temperature was 56 °C for *PjTA-R6*, given its high thermostability, and 37 °C for *CvTA* and *VfTA*. Protein concentrations were the same for all three.

The asymmetric synthesis of aliphatic amines was successful as all ketone substrates were converted by *PjTA-R6* and yielded predominantly (*S*)-amines with all yields exceeding 40% (Table 1). Whereas equilibrium may have been approached in some reactions (e.g., B1 with *PjTA*), the lower

yields with most other substrates and especially in reactions catalyzed by *CvTA* and *VfTA* indicate that differences in yields were mainly determined by kinetics. In particular, amines **A1** and **A2** and branched amines **B1** and **B2** were well synthesized by *PjTA*-R6. Noticeably, using *PjTA*-R6, cyclic amine **C2**, carrying a cyclohexyl group substituent, was better synthesized than **C1**, which has a cyclopropyl group. This suggested that the general bulkiness of the larger substrate did not limit conversion. Chiral analysis of the amines formed by *PjTA*-R6 confirmed the expected (*S*)-enantiioenrichment, and all amines were produced at high enantiomeric excess (e.e.). The enantiopurities of the products indicated a dependence on the difference in size between the large (R_L) and small ($R_S = -CH_3$) side substituents on the carbonyl carbon of the substrates. **A1** ($R_L = -CH_2CH_3$) and **A2** ($R_L = -CH_2CH_2CH_3$) were produced with 94% and 98% e.e., respectively, while all the other amines were produced with >99% e.e.

Under the employed conditions, the yields of straight-chain amines (**A1–A5**) in reactions using *PjTA*-R6 were generally better than those with *CvTA* and *VfTA*. For the production of **A5**, *PjTA*-R6 and *CvTA* displayed comparable results (Table 1). The yields found with *PjTA*-R6 were better in case of straight-chain aliphatic amines with shorter chains (**A1–A2**) than with amines with larger groups (**A3–A5**). In contrast, *VfTA* showed an improving trend in yields with an increasing chain length of the target amines. A previous study on the activity of *VfTA* toward a set of alkyl substrates also showed that the longer the side chain, the higher the activity [27]. For *CvTA*, no such trend was found. For the production of **A1–A3**, *PjTA*-R6 generated higher yields by 28% or more than *CvTA*, while *VfTA* gave the lowest yields. The yields of **A4** and **A5** obtained with the three enzymes differed by less than 11%. The general advantage of asymmetric synthesis using *PjTA*-R6 was also clear from its better enantioselectivity. Whereas *CvTA* and *VfTA* produced linear aliphatic amines with e.e. <94%, all amines formed by *PjAT*-R6 had better than 94% e.e.

For amines with branched carbon chains (**B1–B3**) and cycloalkene groups (**C1–C2**), *PjTA*-R6 generated high product yields, similar to those of amines with linear substituents (Table 1). In particular, **B1** was produced with 95% yield, which was the highest yield obtained with *PjTA*-R6. The advantage of *PjTA*-R6, compared with *CvTA* and *VfTA*, was again apparent from the higher yields. The conversion of amines with nonlinear substituents by *CvTA* and *VfTA* was not successful. This suggests that the presence of a nonlinear large rest group in the substrate prevents proper accommodation of the ketone or subsequent reaction intermediates in these enzymes. Overall, *PjTA*-R6 had a better performance in yield and excellent enantioselectivity, which makes *PjTA*-R6 a promising candidate for the asymmetric amination of aliphatic ketones. The difference between the three enzymes can be due to kinetic and stability effects. Differences observed for the same enzyme should be attributed to kinetic differences, unless conversion is very high when equilibrium may be approached (Table 1, *PjTA*-R6 with **A2** and **B1**). For the branched and cyclic substrates (**B1–B3**, **C1**, and **C2**), which were well converted by *PjTA*-R6 but poorly converted by *CvTA* and *VfTA*, low intrinsic catalytic activity of the latter two enzymes must be the cause of the observed differences.

2.2. Role of Switching Arginine

As mentioned, the native substrate of *PjTA* is the caprolactam biodegradation intermediate 6-aminohexanoic acid (6-AHA) [22]. The crystal structure of *PjTA* complexed with the external aldimine formed from this substrate unveils that the carboxylate group forms a salt bridge with a conserved arginine residue (Arg417) in the large pocket, probably contributing to substrate binding [23]. The arginine side chain switches toward a more outward position upon 6-AHA binding. Arg417 and most surrounding residues were kept during the thermostability engineering that yielded *PjTA*-R6 [24]. During the redesign of other class III (*S*)-selective transaminases, the switching arginine is mostly preserved as amino donors or acceptors often feature a carboxylate functionality [27–29]. However, in *VfTA*, Arg415 has been mutated to open up more space in the large pocket [27,29,30]. For the synthesis of aliphatic alkylamines with IPA as amino donor, neither Arg415 nor Arg417 of *VfTA* and *PjAT*-R6, respectively, are required, and the iminium group can even produce repulsive interactions.

To examine whether Arg417 still has a role in substrate binding when using isopropylamine as amino donor and an amino acceptor substrate lacking a carboxylate functionality, the R417L mutant of *Pj*TA-R6 was prepared and tested in the same reaction scheme as for *Pj*TA-R6. Thermal shift fluorescence assays showed that the thermostability of the R6-R417L enzyme was similar to that of the parent *Pj*TA-R6 ($\Delta T_m^{\text{app}} < 1$ °C). The yields of the enzymatic amination using the mutant R417L remained at the same level as that of *Pj*TA-R6. Yields of **A1** and **A2** obtained with R6-R417L (60% and 69%, respectively) were only slightly lower than that with *Pj*TA-R6 (70% and 80%). As for **A3–A5**, the yields obtained with R6-R417L (54%, 50%, and 47%) were very close to the yields with *Pj*TA-R6. Apparently, the positive charge of the arginine did not hinder activity with the apolar aliphatic acceptors tested here. A possible explanation is conformational flexibility of the aliphatic group of the substrates or of the Arg417, which may avoid close contact with the positively charged iminium function, unlike what is observed in the 6-AHA-bound *Pj*TA structure [23]. We anticipate that Arg417 can be replaced for future engineering needs, e.g., aimed at expanding the binding site for more bulky substrates.

2.3. Structure–Activity Relationship Obtained by Docking

Accommodation of the external aldimine docking complexes formed with different substrates by *Pj*TA-R6 and *Vf*TA were examined to find a structural explanation for the observed activity profiles (Table 1). The substrate-binding pockets of these TAs were positioned at the dimeric interface and consisted of residues from both subunits. Because the small substituent of the tested molecules was always a methyl group, the structure of the binding pocket that accommodates the large substituent was crucial for differences in substrate specificity. The large binding pocket accommodated the carboxyalkyl moiety or large substituent of 6-AHA in *Pj*TA and the phenyl substituent of (*S*)-1-phenylethylamine in *Vf*TA. Structural alignment of *Pj*TA-R6 with *Cv*TA (40% sequence identity, RMSD 1.28 Å) and with *Vf*TA (41% sequence identity, RMSD 1.20 Å) indicated a high overall similarity, although with local differences in the large binding pockets (Figure 1). The side chains of Leu57, Tyr151, Arg417, Met419, Ala230, Trp58, Val260, and Ile261 formed a largely nonpolar binding pocket in *Pj*TA-R6. The corresponding pockets of *Cv*TA and *Vf*TA were also hydrophobic. To examine the features that potentially led to variations in substrate specificities and conferred *Pj*TA-R6 with high reactivity toward a variety of bulky amines, structures of enzyme complexed with product-derived external aldimines were generated by Rosetta docking.

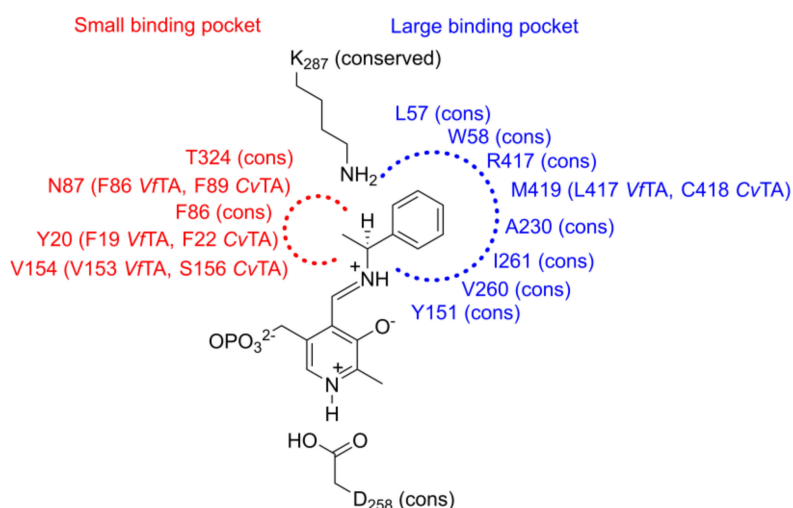


Figure 1. Schematic representation of the binding pocket of *Pj*TA-R6 bearing the external aldimine intermediate (PLP Schiff base with (*S*)-1-phenylethylamine) and comparison of surrounding residues to *Cv*TA and *Vf*TA. The residues in the large binding pocket are in blue. The residues colored red are in the small binding pocket.

The Rosetta interface energies obtained from docking the external aldimine complexes of the 10 different substrates showed a clear correlation with the experimental data observed for both *VfTA* and *PjTA-R6* (Figure 2). Nevertheless, outliers were present in both plots. The most prominent outlier in the *VfTA* dataset was compound **B3**, which exhibited a higher docking score than would be expected based on the experimental yield. **B3** was also one of the three outliers in *PjTA-R6*, along with **A4** and **A5**. The latter two were the only two compounds in the *PjTA-R6* dataset where the switching arginine Arg417 in the docking complex was kept in a crystal-like “out” conformation (discussed later), whereas all the other compounds (**A1–A3**, **B1–B3**, and **C1–C2**) showed Arg417 in an “in” conformation. The lower than expected yield for **A5** with *PjTA-R6* might also be due to the higher concentration of dimethyl sulfoxide (DMSO) used to dissolve this substrate. The correlation between interface energies and experimental yields suggested that structural differences in the binding pockets could have accounted for most of the observed differences in activity within a set of substrates tested with the same enzyme. Because at least one substrate for each enzyme was very well converted, low yields for several substrates, such as **B1–C2** for *CvTA* and *VfTA*, must be due to kinetic causes rather than rapid enzyme inactivation. However, differences in obtained yields between different enzymes might be related to both kinetic and stability differences under the reaction conditions.

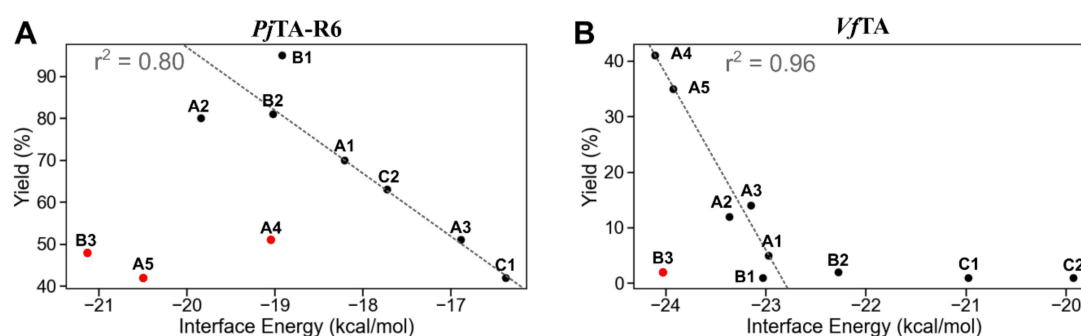


Figure 2. Interface energies of external aldimine complexes show a correlation with the observed activities. (A) *PjTA-R6* and (B) *VfTA*. Outliers (red dots) were not considered for the linear regression (dotted line). For *PjTA-R6*, this means the regression was made using compounds A1, A2, A3, B1, B2, C1, and C2. In the case of *VfTA*, B1, B2, C1, and C2 were not considered for the linear regression as the product was hardly detectable (<2%). The Rosetta interface energy correctly predicted that B2, C1, and C2 would have very low yields; hence, these compounds were not outliers.

The activity data suggested that *PjTA-R6* could accommodate bulkier substituents than *VfTA* (Table 1). The docking simulations revealed that the conformational freedom of the switching arginine played a large role in the ability of *PjTA-R6* to accommodate bulky substrates. In both *VfTA* and *PjTA-R6*, the switching arginine (Arg415 and Arg417, respectively) could adopt one of two conformations that allowed the binding of hydrophobic substituents in the large pocket (Figure 3). We labeled these Arg conformations as “in” and “out” to indicate whether the guanidinium group was pointing inward (toward) the PLP or outward. The “in” and “out” arginine conformations in *VfTA* and *PjTA-R6*, respectively, were crystallized. In the known *VfTA* structures (PDB codes: 4E3Q, 4E3R, 5ZTX, and 3NUI), Arg415 was stabilized in the inward conformation by a hydrogen bond with Trp57. As such, the “in” conformation appeared to be the most stable for the PLP-bound enzyme and the apo-enzyme. On the other hand, the “out” arginine conformation prevailed in the known *PjTA* structures (PDB codes: 6TB1, 6TB0, 6G4B, 6G4C, 6G4D, 6G4E, and 6G4F), where Arg417 was stabilized by electrostatic interactions, either with Ser87 in the wild-type *PjTA* or with Asn87 in *PjTA-R6*. In *PjTA-R6*, Ser87 has been mutated to Asn to improve the enzyme’s thermostability [15,16]. The natural substrate of *PjTA* is 6-AHA, where the role of the switching arginine is to form a salt bridge with the carboxyl group of the substrate (code: 6G4E). *PjTA-R6* and *VfTA* exhibited structurally different “in” and “out” Arg conformations. The outward conformation in *VfTA* placed the Arg415 side chain

in a sandwich-like configuration between Trp57 and Asn53, reducing the ability of Trp57 to freely rotate in response to the presence of a bulky substrate. On the other hand, the “out” conformation of *PjTA*-R6 moved Arg417 away from the binding pocket, locking Arg417 with Asn87 via a polar interaction, thereby both opening up more space in the large pocket and allowing free rotation of Trp58. The inward conformations of Arg415/Arg417 in *VfTA* and *PjTA*-R6 could also account for the difference in reactivity toward bulky substrates. In the “in” conformation, the switching arginine of *PjTA*-R6 made hydrogen bonding contacts with the backbone of Ala230, leaving enough space in the large pocket for bulky substituents. In contrast, *VfTA* locked Arg415 with the indole amino group of Trp57 via hydrogen-bonding interactions, offering less space in the large pocket. Mutations of Trp57 have been carried out, yielding good reactivities toward both alkyl and aromatic substrates [20]. Arg415 from *VfTA* could not reach the backbone of the equivalent Ala228 due to the presence of Leu417, which corresponded to Met419 in *PjTA*-R6. These differences in both the “in” and “out” conformations can explain the distinct catalytic performance of the two enzymes toward bulky substrates.

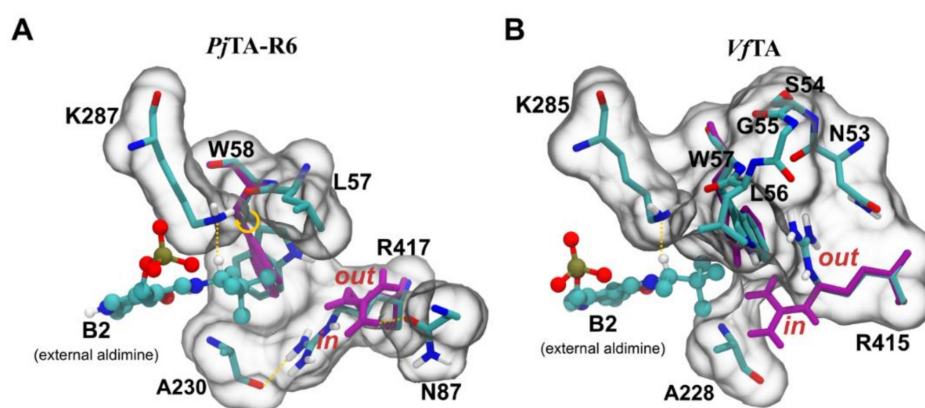


Figure 3. Docked external aldimine structures of 3,3-dimethyl-2-butylamine **B2**, representative of a products with bulky substituents. (A) In *PjTA*-R6, the *tert*-butyl substituent can be easily accommodated in the large pocket by a 40° rotation of Trp58 (yellow arrow). Arg417 does not induce protein–ligand clashes in either the “in” or the “out” orientation. (B) In *VfTA*, both the “in” and the “out” conformations of Arg415 prevent a rotation of Trp57 necessary to accommodate the *tert*-butyl substituent. In both panels, protein structures are shown in licorice representation, and the crystal structure conformations of residues Arg417/Arg415 and Trp58/Trp57 are colored magenta (PDBs 4Q3H for *VfTA* and 6TB1 for *PjTA*-R6). The external aldimine structure of **B2** is shown in CPK representation. Figures were rendered using VMD (Visual Molecular Dynamics).

An additional difference between *PjTA*-R6 and *VfTA* was the effect of increasing the chain length of the alkyl substituent on activity (i.e., substrates **A1**–**A5**). The experimental data showed that longer alkyl substituents negatively impacted conversion by *PjTA*-R6 (Table 1). On the contrary, *VfTA* (and *CvTA*) showed better activities with longer alkyl substituents, as also found by Cho et al. in a study aimed at redesigning the substrate specificity of *VfTA* [27]. Rosetta-generated docking models of the external aldimine intermediates of **A1**–**A5** indicated that *VfTA* accommodated the increasingly longer alkyl chain in the large pocket by pointing the terminal methyl group of the alkyl chain toward the entry tunnel (Figure 4B). In the case of *PjTA*-R6, the equivalent space was partially blocked by Arg417 in both the “in” and “out” conformations. The terminal methyl group of the alkyl chain of **A4** and **A5** was still perfectly able to fit in the large pocket of *PjTA*-R6, albeit less favorably (Figure 4A) than compounds with shorter alkyl substituents (i.e., **A1**–**A3**). The negative effect of Arg417 on the activity of *PjTA*-R6 was minor, as demonstrated by the fact that mutation R417L offered only a marginal improvement in the yields of amines **A4** and **A5**. Furthermore, the large pocket of *PjTA*-R6 contained more polar residues than *VfTA*, thereby offering a less suitable environment to accommodate the lengthening alkyl chain of the **A1**–**A5** series. All in all, while the catalytic activity of *PjTA*-R6 decreased for long alkyl

chains, *Pj*TA-R6 still gave higher yields and higher enantioselectivities than *Vf*TA, making *Pj*TA-R6 valuable for synthesis of enantiopure alkyl amines.

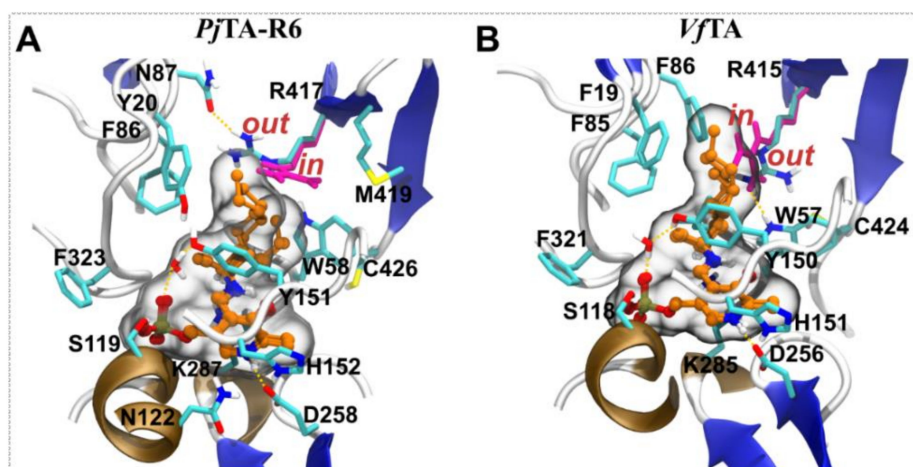


Figure 4. Docking structures of the external aldimine intermediates of amines A1–A5. (A). *Pj*TA-R6 and (B) *Vf*TA. The “out” conformation of the switching arginine is preferred for longer substituents (A4 and A5), whereas the shorter alkyl substituents (A1 to A3) show no preference for either conformation. The large binding site of *Pj*TA-R6 is less hydrophobic than the binding site of *Vf*TA (N87, Y20, and F86 for *Pj*TA-R6 and F86, F19, and F85 for *Vf*TA, respectively). The superimposed external aldimine structures of A1–A5 are shown in CPK representation. The “in” conformation of Arg417/Arg415 is colored magenta.

3. Materials and Methods

3.1. Materials

Isopropylamine, amines (A1–A5, B1–B3, and C1–C2), and the corresponding ketones were purchased from Sigma-Aldrich (St. Louis, MO, USA) or Acros Organics (Fair Lawn, NJ, USA). PLP was purchased from Fisher Scientific (Pittsburgh, PA, USA). Other chemicals were from the same suppliers or Merck Millipore (Burlington, MA, USA).

3.2. Enzyme Expression and Purification

The design, isolation, and properties of the *Pj*TA-R6 mutant have been previously described [24]. The *Pj*TA-R6-R417L mutant was created by QuikChange site-directed mutagenesis. Primers were designed by the QuikChange Primer Design Program of Agilent Technologies (Santa Clara, CA, USA). The mutations were verified by DNA sequencing (Eurofins Genomics, Ebersberg, Germany). After sequencing, the mutated plasmids were transformed into *E. coli* BL21(DE3) for expression. The expression and purification of *Pj*TA-R6, *Pj*TA-R6-R417L, *Cv*TA, and *Vf*TA were performed as previously described. Specific activities of purified enzymes in the deamination of (*S*)-1-phenylethylamine were 47 U/mg (at 70 °C, spectrophotometric acetophenone production assay [24]) or 1.6 and 1.0 U/mg (at 30 °C, coupled enzyme assay using pyruvate as amino acceptor [23]) for *Pj*TA, *Cv*TA, and *Vf*TA, respectively.

3.3. Thermal Shift Assay

Apparent melting temperatures (T_m^{app}) were determined by fluorescence-based thermofluor assay [31]. Specifically, samples of 5 μL 50-fold diluted SYPRO orange and 20 μL 0.5 mg/mL enzyme solution were added to an IQ 96-well PCR plate (Bio-Rad, Hercules, CA, USA) and mixed thoroughly in the wells. The plates were sealed with Microseal B adhesive sealer (Bio-Rad, USA) and heated from 20 to 99 $^{\circ}\text{C}$ in a MyiQ real-time PCR machine (Bio-Rad, USA) with a linear gradient of increasing temperature (1 $^{\circ}\text{C}/\text{min}$). The temperature at the maximum rate of fluorescence change ($d\text{RFU}/dT$) was taken as T_m^{app} [32].

3.4. Amination Reactions and Product Derivatization

Enzyme reactions were carried out in a 1 mL reaction system containing 50 mM potassium phosphate, pH 8.0, with 20 mM ketone substrate, 1 M isopropylamine, 0.5 mM PLP, 1 mg/mL enzyme, and 2% DMSO (20% for **A5**). Reactions were started by addition of substrate and carried out at 56 $^{\circ}\text{C}$ for *Pj*TA-R6 and R417L and 37 $^{\circ}\text{C}$ for *Cv*TA and *Vf*TA over 20 h. Reactions were stopped by adding 200 μL 10 M NaOH, after which 100 μL samples were taken from the basified solutions and extracted once with 300 μL ethyl acetate.

For derivatization, the organic layer was supplied with 300 μL acetic anhydride and 4-dimethylaminopyridine (DMAP) [1], and the solution was shaken at room temperature and 450 rpm for 1 h. Following washing with 500 μL water, the organic layer containing the derivatized product was collected and dried over magnesium sulfate.

3.5. Quantification and Optical Purity

The derivatized products were analyzed by gas chromatography with flame ionization detection on a heptakis-(2,6-di-O-methyl-3-O-pentyl)- β -cyclodextrin column using He at a flow rate of 1 mL/min. The following settings were applied to the analysis of all products and their corresponding commercial references: temperature program: 80 $^{\circ}\text{C}$ for 6.5 min, 10 $^{\circ}\text{C}/\text{min}$ to 160 $^{\circ}\text{C}$, and 20 $^{\circ}\text{C}/\text{min}$ to 200 $^{\circ}\text{C}$ for 10 min; total run time: 26.5 min; inlet temperature: 220 $^{\circ}\text{C}$; and injection volume: 1 μL . To quantify the product, the peaks of the enantiomers were summed up and compared with a commercial amine reference (see Supplementary Materials). To analyze the optical purity of the products, the peaks of different enantiomers were mostly identified with commercial chiral amine references (see Supplementary Materials). The e.e. values were calculated from the peak areas of the (*S*)- and (*R*)-amines.

3.6. Computational Modeling

The coordinates for the (*S*)-amino products of the tested compounds (**A1–A5**, **B1–B3**, and **C1–C2**) were generated in Avogadro (Hanwell et al., 2012; <https://avogadro.cc/>) [26] from their respective SMILES (Simplified Molecular Input Line Entry System) string and optimized by 500 steps of steepest descent energy minimization in the MMFF94 force field. The initial coordinates for the external aldimine forms of the tested substrates were created by superimposing the amino group of the abovementioned (*S*)-amino products to the amino group of the PLP cofactor, whose coordinates were obtained from the crystal structure (PDB: 4E3Q). After superimposition, one of the nitrogen atoms was deleted (the cofactor's), and a covalent bond was added between C4' and the remaining nitrogen atom (the amino substrate's) to form the corresponding Schiff base. A rotamer library for each ligand was generated in YASARA [33]. For each external aldimine structure, 1000 rotamers were generated by random perturbation of the heavy-atom dihedrals (*SampleDih* YASARA routine) while maintaining the cofactor atoms frozen. Pairwise RMSD (root-mean-square deviation) between all rotamers within each library was used for selecting unique rotamers (cutoff $<0.05 \text{ \AA}$), resulting in 200–300 unique rotamers for each ligand.

Structure coordinates for *PjTA*-R6 [24] and *VfTA* [30] were obtained from the PDB databank (6TB1 and 4E3Q, respectively). The crystal structures were prepared for docking by first implementing the *CleanObj* YASARA routine, which added explicit hydrogens to the structure, and converting Se-Met residues into canonical Met. Protonation states of residues Asp, Glu, His, and Lys were calculated by an automatic YASARA routine at pH 7 [33]. The resulting scaffold structure was stripped of any nonprotein residues.

The scaffold protein structure was relaxed by the Rosetta (v2020.11) Relax [34] algorithm with the following command-line arguments: `-ignore_unrecognized_res, -relax:constrain_relax_to_start_coords, -relax:coord_constrain_sidechains, -relax:ramp_constraints false, -use_input_sc, -correct, -no_his_his_pairE, -no_optH false, -flip_HNQ`. Binding poses of external aldimine complexes were generated using the Rosetta Enzyme Design application [35]. One randomly selected rotamer from each conformer library was overlapped to the binding site (subunit A) of *PjTA*-R6 or *VfTA* by RMSD alignment to the cofactor heavy atoms. The resulting structure served as input for the docking calculations. During the docking simulations, residues with C α closer than 10 Å from any ligand heavy atom were allowed to repack. For *PjTA*-R6, residues 20, 87, 59, 118, 119, 151, 152, 225, 259, 287, 292, and 324 were set to NATRO (natural rotamer, kept fixed). For *VfTA*, residues 19, 53, 115, 118, 121, 150, 151, 256, 258, and 322 were set to NATRO. No constraints were used in the production runs. Additionally, the following command-line arguments were used for the Rosetta docking: `-enzdes, -cst_predock, -cst_design, -cut1 0.0 -cut2 0.0, -cut3 8.0, -cut4 10.0, -cst_min, -chi_min, -bb_min, -packing::use_input_sc, -packing::soft_rep_design, -design_min_cycles 3, -ex1:level 4, -ex1:level 4, -ex1aro:level 4, -ex2aro:level 4`. A total of 200 docking complexes were generated for each ligand, and the average interface energies were computed and compared against the experimental yield. Figures were generated using VMD (<http://www.ks.uiuc.edu/Research/vmd/>).

4. Conclusions

PjTA-R6 was capable of converting various aliphatic ketones into the corresponding amines with good activity, including when compared to *CvTA* and *VfTA*. The scope of aliphatic amines that can be asymmetrically synthesized spans from amines with linear (**A1–A5**) or branched substituents (**B1–B3**) to lesser studied amines with a cycloalkyl moiety (**C1–C2**). The enantioselectivity of *PjTA*-R6 was ideal for most cases, which plays in favor of using this enzyme for chiral amine production. *PjTA*-R6 catalyzed amination at a relatively high temperature (56 °C). Its robustness allows use of the enzyme under beneficial conditions for enzymatic amination, e.g., high temperature, higher amino donor concentration, and presence of cosolvent for better substrate and product solubility. The mutant R6-R417L showed a comparable performance to *PjTA*-R6, indicating that the switching arginine Arg417 is replaceable when a carboxylate functionality is absent from the keto substrate and the amino donor.

The interface energies obtained with Rosetta docking simulations of the external aldimine reaction intermediates showed a clear correlation with yield in amine synthesis, both in case of *PjTA*-R6 and *VfTA*. Further comparison of the docked structures unveiled differences in the conformations of the switching arginine that interacts with the native substrates of *PjTA*-R6 and *VfTA*. In *VfTA*, the conformational freedom of the switching arginine is more restricted than in *PjTA*-R6 and does not allow *VfTA* to accommodate bulky substrates. Overall, the binding site of *PjTA*-R6 is better at adapting to fit bulkier substituents than the related enzyme *VfTA*. The observation that the relative reactivity of *PjTA*-R6 can be rationalized by docking simulations and energy calculations suggests that these computational tools can support the design of variants with expanded or shifted substrate spectrum, which is important for furthering applicability in green chemistry.

Supplementary Materials: The following are available online at <http://www.mdpi.com/2073-4344/10/11/1310/s1>, Figure S1: The chromatograms of 20, 2, and 0.2 mM **A3** sample after derivatization; Figure S2: Representative chromatogram of *PjTA*-R6-catalyzed transamination of 2-butanone yielding sec-butylamine (**A1**) after product derivatization; Figure S3: Representative chromatogram of *PjTA*-R6-catalyzed transamination of 2-pentanone yielding 2-aminopentane (**A2**) after product derivatization; Figure S4: Representative chromatogram of *PjTA*-R6-catalyzed transamination of 2-hexanone yielding 2-aminohexane (**A3**) after product derivatization.

Figure S5: Representative chromatogram of *Pj*TA-R6-catalyzed transamination of 2-heptanone yielding 2-aminoheptane (**A4**) after product derivatization; Figure S6: Representative chromatogram of *Pj*TA-R6-catalyzed transamination of 2-octanone yielding 2-aminooctane (**A5**) after product derivatization; Figure S7: Representative chromatogram of *Pj*TA-R6-catalyzed transamination of 3-methyl-2-butanone yielding 3-methyl-2-butanamine (**B1**) after product derivatization; Figure S8: Representative chromatogram of *Pj*TA-R6-catalyzed transamination of 3,3-dimethyl-2-butanone yielding 3,3-dimethyl-2-butanamine (**B2**) after product derivatization; Figure S9: Representative chromatogram of *Pj*TA-R6-catalyzed transamination of 4-methyl-2-pentanone yielding 4-methyl-2-pentanamine (**B3**) after product derivatization; Figure S10: Representative chromatogram of *Pj*TA-R6-catalyzed transamination of 1-cyclopropylethanone yielding 1-cyclopropylethanamine (**C1**) after product derivatization; Figure S11: Representative chromatogram of *Pj*TA-R6-catalyzed transamination of 1-cyclohexylethanone yielding 1-cyclohexylethanamine (**C2**) after product derivatization; Figure S12: SDS-PAGE analysis of purified *Cv*TA, *Vf*TA, and *Pj*TA-R6; Table S1: The retention times of the derivatized products.

Author Contributions: Conceptualization, Q.M., C.R.-P., H.J.W., S.J.M., and D.B.J.; formal analysis, L.D. and C.R.-P.; funding acquisition, Q.M., C.R.-P., L.D., S.J.M., and D.B.J.; investigation, L.D., C.R.-P., and Q.M.; methodology, L.D., Q.M., and C.R.-P.; supervision, H.J.W., S.J.M., and D.B.J.; validation, Q.M. and C.R.-P.; visualization, L.D., C.R.-P., and Q.M.; writing—original draft, L.D., Q.M., and C.R.-P.; writing—review and editing, H.J.W., S.J.M., and D.B.J. All authors have read and agreed to the published version of the manuscript.

Funding: The research of H.J.W. was supported by the Dutch Ministry of Economic Affairs through BE-Basic, grant FS02.005.

Acknowledgments: L.D. thanks the University of Groningen and Jilin University for the scholarships they provided. Q.M. thanks the China Scholarship Council for a PhD fellowship. C.R.P. thanks CONACYT for the doctoral fellowship.

Conflicts of Interest: The authors declare no conflict of interest.

References

1. Koszelewski, D.; Lavandera, I.; Clay, D.; Rozzell, D.; Kroutil, W. Asymmetric Synthesis of Optically Pure Pharmacologically Relevant Amines Employing ω -Transaminases. *Adv. Synth. Catal.* **2008**, *350*, 2761–2766. [[CrossRef](#)]
2. Ghislieri, D.; Turner, N.J. Biocatalytic Approaches to the Synthesis of Enantiomerically Pure Chiral Amines. *Top. Catal.* **2014**, *57*, 284–300. [[CrossRef](#)]
3. Patil, M.D.; Grogan, G.; Bommarius, A.; Yun, H. Recent Advances in ω -Transaminase-Mediated Biocatalysis for the Enantioselective Synthesis of Chiral Amines. *Catalysts* **2018**, *8*, 254. [[CrossRef](#)]
4. Rösler, M.; Anand, R.; Cicin-Sain, A.; Gauthier, S.; Agid, Y.; Dal-Bianco, P.; Stähelin, H.B.; Hartman, R. Efficacy and safety of rivastigmine in patients with Alzheimer’s disease: International randomised controlled trial. *BMJ* **1999**, *318*, 8. [[CrossRef](#)] [[PubMed](#)]
5. Hoye, T.R.; Chen, M. Total synthesis of (ent)-korupensamine D. *Tetrahedron Lett.* **1996**, *37*, 3099–3100. [[CrossRef](#)]
6. Chen, X.; Chen, J.; De Paolis, M.; Zhu, J. Synthetic Studies toward Ecteinascidin 743. *J. Org. Chem.* **2005**, *70*, 4397–4408. [[CrossRef](#)]
7. Kelly, S.A.; Pohle, S.; Wharry, S.; Mix, S.; Allen, C.C.R.; Moody, T.S.; Gilmore, B.F. Application of ω -Transaminases in the Pharmaceutical Industry. *Chem. Rev.* **2018**, *118*, 349–367. [[CrossRef](#)]
8. Simon, R.C.; Richter, N.; Busto, E.; Kroutil, W. Recent Developments of Cascade Reactions Involving ω -Transaminases. *ACS Catal.* **2014**, *4*, 129–143. [[CrossRef](#)]
9. Eliot, A.C.; Kirsch, J.F. Pyridoxal Phosphate Enzymes: Mechanistic, Structural, and Evolutionary Considerations. *Annu. Rev. Biochem.* **2004**, *73*, 383–415. [[CrossRef](#)]
10. Slabu, I.; Galman, J.L.; Lloyd, R.C.; Turner, N.J. Discovery, Engineering, and Synthetic Application of Transaminase Biocatalysts. *ACS Catal.* **2017**, *7*, 8263–8284. [[CrossRef](#)]
11. Voss, M.; Das, D.; Genz, M.; Kumar, A.; Kulkarni, N.; Kustoscz, J.; Kumar, P.; Bornscheuer, U.T.; Höhne, M. In Silico Based Engineering Approach to Improve Transaminases for the Conversion of Bulky Substrates. *ACS Catal.* **2018**, *8*, 11524–11533. [[CrossRef](#)]
12. Han, S.-W.; Kim, J.; Cho, H.-S.; Shin, J.-S. Active Site Engineering of ω -Transaminase Guided by Docking Orientation Analysis and Virtual Activity Screening. *ACS Catal.* **2017**, *7*, 3752–3762. [[CrossRef](#)]
13. Sirin, S.; Kumar, R.; Martinez, C.; Karmilowicz, M.J.; Ghosh, P.; Abramov, Y.A.; Martin, V.; Sherman, W. A Computational Approach to Enzyme Design: Predicting ω -Aminotransferase Catalytic Activity Using Docking and MM-GBSA Scoring. *J. Chem. Inf. Model.* **2014**, *54*, 2334–2346. [[CrossRef](#)] [[PubMed](#)]

14. Dourado, D.F.A.R.; Pohle, S.; Carvalho, A.T.P.; Dheeman, D.S.; Caswell, J.M.; Skvortsov, T.; Miskelly, I.; Brown, R.T.; Quinn, D.J.; Allen, C.C.R.; et al. Rational Design of a (S)-Selective-Transaminase for Asymmetric Synthesis of (1S)-1-(1,1'-biphenyl-2-yl)ethanamine. *ACS Catal.* **2016**, *6*, 7749–7759. [[CrossRef](#)]
15. Cassimjee, K.E.; Manta, B.; Himo, F. A quantum chemical study of the ω -transaminase reaction mechanism. *Org. Biomol. Chem.* **2015**, *13*, 8453–8464. [[CrossRef](#)]
16. Koszelewski, D.; Tauber, K.; Faber, K.; Kroutil, W. ω -Transaminases for the synthesis of non-racemic α -chiral primary amines. *Trends Biotechnol.* **2010**, *28*, 324–332. [[CrossRef](#)]
17. Park, E.-S.; Malik, M.S.; Dong, J.-Y.; Shin, J.-S. One-Pot Production of Enantiopure Alkylamines and Arylalkylamines of Opposite Chirality Catalyzed by ω -Transaminase. *ChemCatChem* **2013**, *5*, 1734–1738. [[CrossRef](#)]
18. Liu, T.-L.; Wang, C.-J.; Zhang, X. Synthesis of Chiral Aliphatic Amines through Asymmetric Hydrogenation. *Angew. Chem. Int. Ed.* **2013**, *52*, 8416–8419. [[CrossRef](#)]
19. Shin, J.-S.; Kim, B.-G. Asymmetric Synthesis of Chiral Amines with ω -Transaminase. *Biotechnol. Bioeng.* **1999**, *65*, 206–211. [[CrossRef](#)]
20. Fuchs, M.; Farnberger, J.E.; Kroutil, W. The Industrial Age of Biocatalytic Transamination: The Industrial Age of Biocatalytic Transamination. *Eur. J. Org. Chem.* **2015**, *2015*, 6965–6982. [[CrossRef](#)]
21. Tufvesson, P.; Lima-Ramos, J.; Jensen, J.S.; Al-Haque, N.; Neto, W.; Woodley, J.M. Process considerations for the asymmetric synthesis of chiral amines using transaminases. *Biotechnol. Bioeng.* **2011**, *108*, 1479–1493. [[CrossRef](#)]
22. Otzen, M.; Palacio, C.; Janssen, D.B. Characterization of the caprolactam degradation pathway in *Pseudomonas jessenii* using mass spectrometry-based proteomics. *Appl. Microbiol. Biotechnol.* **2018**, *102*, 6699–6711. [[CrossRef](#)] [[PubMed](#)]
23. Palacio, C.M.; Rozeboom, H.J.; Lanfranchi, E.; Meng, Q.; Otzen, M.; Janssen, D.B. Biochemical properties of a *Pseudomonas* aminotransferase involved in caprolactam metabolism. *FEBS J.* **2019**, *286*, 4086–4102. [[CrossRef](#)] [[PubMed](#)]
24. Meng, Q.; Capra, N.; Palacio, C.M.; Lanfranchi, E.; Otzen, M.; van Schie, L.Z.; Rozeboom, H.J.; Thunnissen, A.-M.W.H.; Wijma, H.J.; Janssen, D.B. Robust ω -Transaminases by Computational Stabilization of the Subunit Interface. *ACS Catal.* **2020**, *10*, 2915–2928. [[CrossRef](#)]
25. Calvelage, S.; Dörr, M.; Höhne, M.; Bornscheuer, U.T. A Systematic Analysis of the Substrate Scope of (S)- and (R)-Selective Amine Transaminases. *Adv. Synth. Catal.* **2017**, *359*, 4235–4243. [[CrossRef](#)]
26. Huisman, G.W.; Collier, S.J. On the development of new biocatalytic processes for practical pharmaceutical synthesis. *Curr. Opin. Chem. Biol.* **2013**, *17*, 284–292. [[CrossRef](#)] [[PubMed](#)]
27. Cho, B.-K.; Park, H.-Y.; Seo, J.-H.; Kim, J.; Kang, T.-J.; Lee, B.-S.; Kim, B.-G. Redesigning the substrate specificity of ω -aminotransferase for the kinetic resolution of aliphatic chiral amines. *Biotechnol. Bioeng.* **2008**, *99*, 275–284. [[CrossRef](#)] [[PubMed](#)]
28. Nobili, A.; Steffen-Munsberg, F.; Kohls, H.; Trentin, I.; Schulzke, C.; Höhne, M.; Bornscheuer, U.T. Engineering the Active Site of the Amine Transaminase from *Vibrio fluvialis* for the Asymmetric Synthesis of Aryl-Alkyl Amines and Amino Alcohols. *ChemCatChem* **2015**, *7*, 757–760. [[CrossRef](#)]
29. Genz, M.; Melse, O.; Schmidt, S.; Vickers, C.; Dörr, M.; van den Bergh, T.; Joosten, H.-J.; Bornscheuer, U.T. Engineering the Amine Transaminase from *Vibrio fluvialis* towards Branched-Chain Substrates. *ChemCatChem* **2016**, *8*, 3199–3202. [[CrossRef](#)]
30. Midelfort, K.S.; Kumar, R.; Han, S.; Karmilowicz, M.J.; McConnell, K.; Gehlhaar, D.K.; Mistry, A.; Chang, J.S.; Anderson, M.; Villalobos, A.; et al. Redesigning and characterizing the substrate specificity and activity of *Vibrio fluvialis* aminotransferase for the synthesis of imagabalin. *Protein Eng. Des. Sel.* **2013**, *26*, 25–33. [[CrossRef](#)]
31. Ericsson, U.B.; Hallberg, B.M.; DeTitta, G.T.; Dekker, N.; Nordlund, P. Thermofluor-based high-throughput stability optimization of proteins for structural studies. *Anal. Biochem.* **2006**, *357*, 289–298. [[CrossRef](#)] [[PubMed](#)]
32. Boivin, S.; Kozak, S.; Meijers, R. Optimization of protein purification and characterization using Thermofluor screens. *Protein Expr. Purif.* **2013**, *91*, 192–206. [[CrossRef](#)] [[PubMed](#)]
33. Krieger, E.; Vriend, G. YASARA View—Molecular Graphics for 1139 all Devices—from Smartphones to Workstations. *Bioinformatics* **2014**, *30*, 2981–2982. [[CrossRef](#)] [[PubMed](#)]

34. Conway, P.; Tyka, M.D.; DiMaio, F.; Konerding, D.E.; Baker, D. Relaxation of backbone bond geometry improves protein energy landscape modeling. *Protein Sci.* **2014**, *23*, 47–55. [[CrossRef](#)] [[PubMed](#)]
35. Richter, F.; Leaver-Fay, A.; Khare, S.D.; Bjelic, S.; Baker, D. De Novo Enzyme Design using Rosetta3. *PLoS ONE* **2011**, *6*, e19230. [[CrossRef](#)]

Publisher's Note: MDPI stays neutral with regard to jurisdictional claims in published maps and institutional affiliations.



© 2020 by the authors. Licensee MDPI, Basel, Switzerland. This article is an open access article distributed under the terms and conditions of the Creative Commons Attribution (CC BY) license (<http://creativecommons.org/licenses/by/4.0/>).